VIP Dehydrogenation Very Important Paper

Deutsche Ausgabe: DOI: 10.1002/ange.201507119
Internationale Ausgabe: DOI: 10.1002/anie.201507119

Al_2O_3 Nanosheets Rich in Pentacoordinate Al^{3+} Ions Stabilize Pt-Sn Clusters for Propane Dehydrogenation

*Lei Shi, Gao-Ming Deng, Wen-Cui Li, Shu Miao, Qing-Nan Wang, Wei-Ping Zhang, and An-Hui Lu**

Abstract: *In heterogeneous catalysis, supports play a crucial role in modulating the geometric and electronic structure of the active metal phase for optimizing the catalytic performance. A γ-Al_2O_3 nanosheet that contains 27% pentacoordinate Al^{3+} sites can nicely disperse and stabilize raft-like Pt-Sn clusters as a result of strong interactions between metal and support. Consequently, there are strong electronic interactions between the Pt and Sn atoms, resulting in an increase in the electron density of the Pt sites. When used in the propane dehydrogenation reaction, this catalyst displayed an excellent specific activity for propylene formation with >99% selectivity, and superior anti-coking and anti-sintering properties. Its exceptional ability to maintain the high activity and stability at ultrahigh space velocities further showed that the sheet construction of the catalyst facilitated the kinetic transfer process.*

The dehydrogenation of propane (DHP) to propylene represents an economical and environmentally friendly route compared to the traditional thermal or catalytic cracking of crude-oil-derived naphtha, which requires large amounts of energy and generates enormous CO_2 emissions.[1] An alumina-supported Pt catalyst is a vital component of the DHP process owing to its superior ability to activate paraffinic C–H bonds and its low activity in C–C bond cleavage. Further addition of a Sn promoter has proved necessary to obtain the optimum catalyst.[2] Nevertheless, the fast deactivation of the catalyst by coke deposition or Pt sintering is still a major problem.[3] During the DHP process, coke formation generally occurs as a result of side reactions, such as hydrogenolysis, cracking, and isomerization, that are sensitive to the Pt particle size.[4] Therefore, the use of smaller Pt particles can effectively inhibit coke formation. Alternatively, increasing the electron density on the Pt atoms can also effectively weaken the adsorption of alkene molecules and coke precursors, thus reducing coke deposition.[5]

The catalyst support plays a crucial role in modulating the geometric and electronic structure of active metal phases for optimizing the catalytic activity, selectivity, and stability. In the case of Al_2O_3 supports, the coordinatively unsaturated aluminum atoms have a great impact on the anchoring Pt atoms and on maintaining high stability.[6] From a kinetics point of view, thin, sheet-like nanoarchitectures are an ideal choice for improving the mass-transfer and diffusion kinetics,[7] which can in principle inhibit the secondary reaction that generates coke. However, owing to the structural complexity and our poor understanding of the crystalline structures of Al_2O_3, it is still challenging to precisely tailor the structure of Al_2O_3 for optimizing the catalyst performance.[8]

Herein, a highly active and stable $PtSn/Al_2O_3$ sheet catalyst for the DHP reaction has been synthesized, using γ-Al_2O_3 nanosheets as a support that is rich in pentacoordinate Al^{3+} ions. Such Al_2O_3 nanosheets perform extremely well in dispersing and stabilizing raft-like Pt-Sn clusters. The electronic interactions between the two metals and the electron densities of the Pt sites are thus increased. Together with the improved diffusion kinetics caused by the nanosheet structure, these properties simultaneously and substantially increase the catalytic reactivity and especially the catalyst stability in the DHP reaction.

A transmission electron microscopy (TEM) image of the $PtSn/Al_2O_3$ sheet catalyst shows its sheet-like morphology with distinct surface roughness (Figure 1A). Aberration-corrected HAADF-STEM images show that small discrete clusters, with sizes ranging from 0.9–1.6 nm and a mean diameter of 1.3 nm, are homogenously distributed on the surface of the Al_2O_3 nanosheet (Figure 1B,C). A higher-magnification STEM image reveals that these clusters are tightly attached to the surface of the Al_2O_3 nanosheet, indicating a strong interaction between metal and support (Figure 1D). A small number of isolated atoms and dimers or trimers were also observed, as shown in the magnified area (Figure 1E). The intensity profiles of the close-up images (Figure 1F,G) show that the annular dark-field intensities of clusters along the F direction in Figure 1E are 1 to 1.5 times higher than that of an individual atom in the G direction, indicating that the cluster consists of a stack with a thickness of less than two atoms.[9] A further H_2/O_2 titration measurement (Supporting Information, Table S1) showed that the dispersity of Pt is close to 100%, suggesting that almost all of the Pt atoms are exposed on the surface. These results nicely support the conclusion that the clusters on the Al_2O_3 nanosheet have a raft-like structure and experience strong metal–

[*] Dr. L. Shi, G.-M. Deng, Prof. W.-C. Li, Q.-N. Wang, Prof. W.-P. Zhang, Prof. A.-H. Lu
State Key Laboratory of Fine Chemicals
School of Chemical Engineering
Dalian University of Technology
Dalian 116024 (P. R. China)
E-mail: anhuilu@dlut.edu.cn
Dr. S. Miao
Dalian National Laboratory of Clean Energy
Dalian Institute of Chemical Physics
Chinese Academy of Sciences
Dalian 116023 (P. R. China)

Supporting information for this article is available on the WWW under http://dx.doi.org/10.1002/anie.201507119.

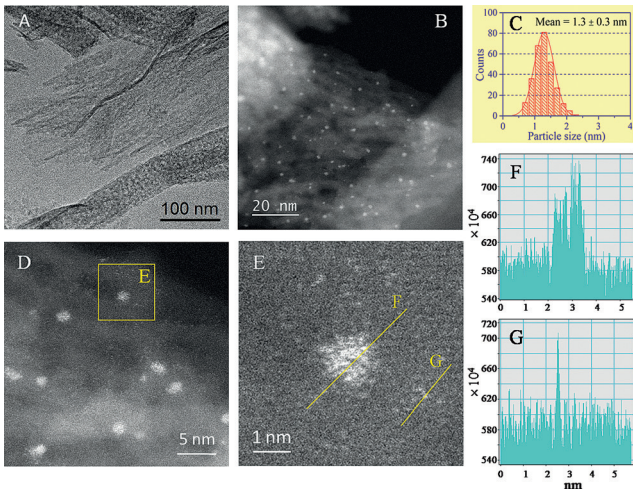

Figure 1. A) TEM image. B, D, E) HAADF-STEM images. C) Size distribution of the metal clusters. F, G) Normalized image intensities in the F and G directions of the $PtSn/Al_2O_3$ sheet catalyst.

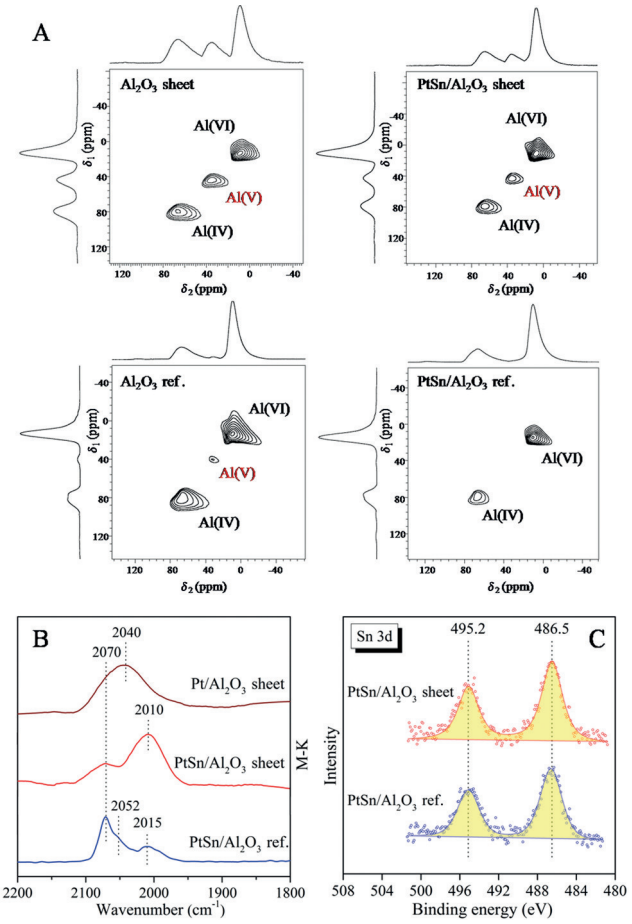

Figure 2. A) Two-dimensional ^{27}Al MQ MAS NMR spectra, B) CO DRIFT spectra, and C) Sn 3d XPS spectra of the catalysts.

support interactions. Energy-dispersive X-ray (EDX) element mapping analysis (Figure S1) visually confirmed that the clusters on the Al_2O_3 nanosheets consist of both Pt and Sn atoms. All of these observations suggest that the γ-Al_2O_3 nanosheet is an excellent support for dispersing and stabilizing raft-like Pt-Sn clusters because of the strong metal–support interactions.

For the γ-Al_2O_3 nanosheets, several XRD diffraction peaks, namely (222), (311), and (511), that are sensitive to the Al^{3+} distribution[8c] are extremely weak or even absent (Figure S2), indicating a high degree of Al^{3+} disorder. To obtain a definitive picture of the local structure of the Al^{3+} cations, the nanosheets were analyzed by two-dimensional ^{27}Al multiple-quantum magic angle spinning (MQ MAS) NMR spectroscopy. As shown in Figure 2 A, three distinct Al species were observed for the Al_2O_3 sheet and $PtSn/Al_2O_3$ sheet samples. The isotropic chemical shifts (δ_{iso}, Table S2) of 11 ppm and 74 ppm represent Al^{3+} ions with octahedral [Al(VI)] and tetrahedral [Al(IV)] coordination geometries, respectively.[10] The resonance at approximately 41 ppm was attributed to unsaturated Al^{3+} cations with pentahedral coordination [Al(V)].[11] It is generally accepted that surface Al^{3+} centers with unsaturated coordination are the important anchoring sites for maintaining the high dispersion and thermal stability of the catalytically active phase.[6] The Al_2O_3 nanosheet synthesized in this work contains a large percentage (27%) of pentacoordinate Al^{3+} sites (Figure S3). This unique structure could account for the formation of the highly dispersed and stabilized Pt-Sn clusters on its surface.

To further clarify the effect of unsaturated Al^{3+} sites on the structure of the supported Pt-Sn clusters, a commercial γ-Al_2O_3 carrier (denoted Al_2O_3 ref., Alfa Aesar) with only few (5%) pentacoordinate Al^{3+} sites (Figure 2 A, Figure S3) was chosen for comparative studies and loaded with Pt and Sn using the same preparation procedure as for our $PtSn/Al_2O_3$ sheet. Instead of the complete dispersion of PtSn on the Al_2O_3 sheet surface, TEM images of the $PtSn/Al_2O_3$ ref. catalyst revealed the presence of a considerable number of three-dimensional nanoparticles with sizes of 2 to 3 nm (Figure S4). H_2/O_2 titration analysis revealed a lower Pt dispersity (Table S1), which is consistent with the TEM results. These data clearly demonstrate that the dispersion state and the morphology of the Pt-Sn active phase are strongly affected by the interaction with unsaturated Al(V) sites.

As mentioned previously, the electronic states of active phases are another crucial factor that influences the catalytic behavior.[12] DRIFT spectroscopy with CO as the probe was used to investigate the local electronic environment of Pt. As shown in Figure 2 B, the adsorption of CO on the Pt/Al_2O_3 sheet catalyst produced a vibration at 2040 cm^{-1} and a visible shoulder at 2070 cm^{-1}. The former can be assigned to the linear adsorption of CO on Pt sites with saturated coordination, whereas the latter corresponds to coordinatively unsaturated Pt sites.[13] For the $PtSn/Al_2O_3$ sheet catalyst, a new and strong band appeared at 2010 cm^{-1} while the band at 2040 cm^{-1} vanished.

It was previously reported that Sn was more inclined to selectively cover low-coordination Pt sites in the Pt-Sn system.[14] Given that the Sn addition is the only difference, such a change in the C–O vibration frequency must originate from the interaction of Pt and Sn species. Metallic Sn or Sn^{2+} species in close contact with Pt are able to transfer electrons to the 5d band of Pt.[5] Combining the results of the Sn 3d XPS

(Figure 2C) and the temperature-programmed reduction by hydrogen (H_2-TPR; Figure S5), it could be confirmed that Sn is mainly present in the +2 valence state in the $PtSn/Al_2O_3$ sheet catalyst.[15] All of these results, especially the new band at 2010 cm^{-1} and the disappearance of the vibration at 2040 cm^{-1} in the CO DRIFT spectra, directly corroborate the hypothesis that there are strong electronic interactions between Pt and Sn in the $PtSn/Al_2O_3$ sheet catalyst, while the reduced frequency of the C–O vibration clearly demonstrates an increase in the electron density on Pt. On the other hand, CO DRIFT spectroscopy of the $PtSn/Al_2O_3$ ref. catalyst revealed a strong vibration band at 2070 cm^{-1} and a small vibration at 2015 cm^{-1}, suggesting that Pt and Sn only weakly interact in this reference catalyst. By comparing the Sn/Al(V) ratios (Table S2) and H_2 consumption (Figure S5) of the two catalysts during reduction, it was confirmed that Sn can maintain a higher dispersion on the surface of the Al_2O_3 sheet. Therefore, in this sheet catalyst, the probability for a Sn species to be located in close proximity to a Pt species is high, which leads to the stronger electronic interactions. These SnO promoter interactions will further help to disperse and stabilize the tiny Pt clusters, especially during the course of reactions. Overall, these geometric and electronic features are very attractive for a dehydrogenation catalyst with excellent catalytic reactivity and stability.

The propane dehydrogenation reaction was investigated under atmospheric pressure at 590 °C. As shown in Figure 3A, the initial conversion of propane on the $PtSn/Al_2O_3$ sheet catalyst was 48.7 % at a space velocity (WHSV) of 9.4 h^{-1} near equilibrium (50 %) in a feed of 16.2 kPa C_3H_8, 20.3 kPa H_2, and N_2 balance. After 24 h, the dehydrogenation reaction showed a very small decrease in conversion of 0.17 % per hour, suggesting that only slight deactivation had occurred. Meanwhile, the propylene selectivity was as high as 99.1 % after a 24 h test. On the other hand, for the $PtSn/Al_2O_3$ reference catalyst, propane conversion dramatically dropped from an initial 43.8 % to 28.3 % after 24 h. The propylene selectivity was also lower than for the $PtSn/Al_2O_3$ sheet catalyst. A first-order deactivation model was used to evaluate the catalyst stability (for details, see the Supporting Information).[16] As shown in Table S3, a low deactivation rate of 0.007 h^{-1} and a catalyst life time of 143 h for the $PtSn/Al_2O_3$ sheet catalyst quantitatively demonstrate its high stability compared to the $PtSn/Al_2O_3$ ref. catalyst (0.026 h^{-1}, 38 h). The propylene yields of these two PtSn-based catalysts and previously developed catalysts are compared as a function of the deactivation rate in Figure 3B. The best yield at a low k_d value clearly demonstrates the superior reactivity and stability of the $PtSn/Al_2O_3$ sheet catalyst in the DHP reaction. To optimize its dehydrogenation performance, the WHSV effect was further investigated. As shown in Figure 3C and Table S3, when an ultra-high WHSV of 56.5 h^{-1} was used, a very high specific rate (i.e., the moles of C_3H_6 formed per mole of Pt per second) of 5.36 s^{-1} and a low deactivation rate (0.014 h^{-1}) were achieved with the $PtSn/Al_2O_3$ sheet catalyst; these values are superior to those of state-of-the-art Pt-based dehydrogenation catalysts (Tables S3 and S4).[2]

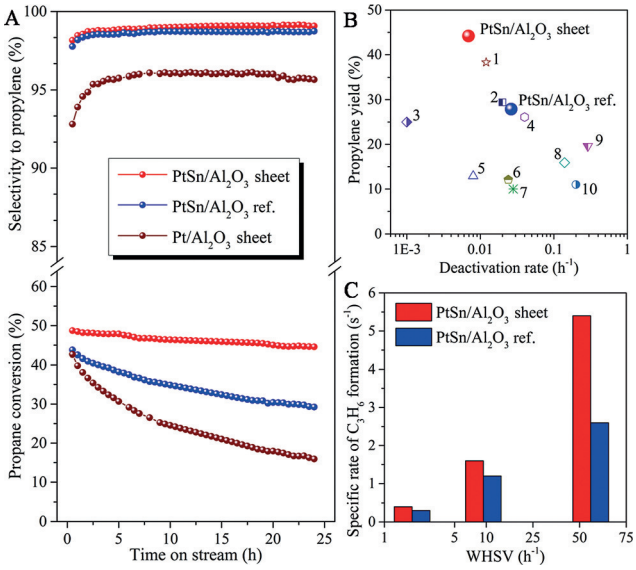

Figure 3. A) Conversion and selectivity as a function of time during propane dehydrogenation. B) Yield versus deactivation rate for the catalysts described in this work and in the literature (1–10, see Table S4). C) Specific rate of C_3H_6 formation versus WHSV for two types of $PtSn/Al_2O_3$ catalyst.

It is important to note that the 2D sheet structure might promote diffusion and thereby influence the catalytic behavior in the DHP reaction. When higher space velocities are used, the effects of mass transfer and diffusion on the reaction rate will be more obvious. The increase in the specific activity of the $PtSn/Al_2O_3$ sheet catalyst was substantially larger than that of the $PtSn/Al_2O_3$ ref. catalyst when the WHSV was increased from 1.9 h^{-1} to 56.5 h^{-1} (Figure 3C). This trend reveals that the sheet-like construction of the catalyst has a great impact on the catalyzed reactions, mostly likely by accelerating mass transfer and diffusion and, possibly, by allowing easy heat transfer. From the kinetics point of view, these results nicely confirm the promoting role of this nanosheet catalyst in the DHP reaction.

Characterization of the spent catalysts was performed to shed further light on the correlation between the high reaction rate and stability of the $PtSn/Al_2O_3$ sheet catalyst and its structure. STEM analysis (Figure 4A,B) showed that the size and morphology of Pt-Sn clusters supported on the Al_2O_3 sheet had undergone negligible changes even after a 24 h dehydrogenation reaction, which demonstrates the excellent sintering resistance of this catalyst. As mentioned earlier, coke deposition during propane dehydrogenation is another main cause of catalyst deactivation;[2] therefore, the amount, type, and location of the coke formed on the two Pt-Sn catalysts were studied. As shown in Figure 4C, the amount (3.7 %) of coke deposited on the $PtSn/Al_2O_3$ sheet was much lower than on the $PtSn/Al_2O_3$ ref. (7.6 %) catalyst. A comparison of the intensity ratios ($I_{D1}/I_G = 0.85$ vs. 0.79, $A_D/A_G = 3.11$ vs. 2.92) of the D to G bands in the Raman spectra (Figure 4D) of the $PtSn/Al_2O_3$ sheet and $PtSn/Al_2O_3$ ref. catalysts suggests that the coke on the surface of the former is more amorphous.[17] The TPO profiles (Figure 4C) of the two spent catalysts reveal that most of the coke is located on the support surface.[18] Pt dispersion measurements (Table S1) for the spent catalysts further imply that the proportion of active

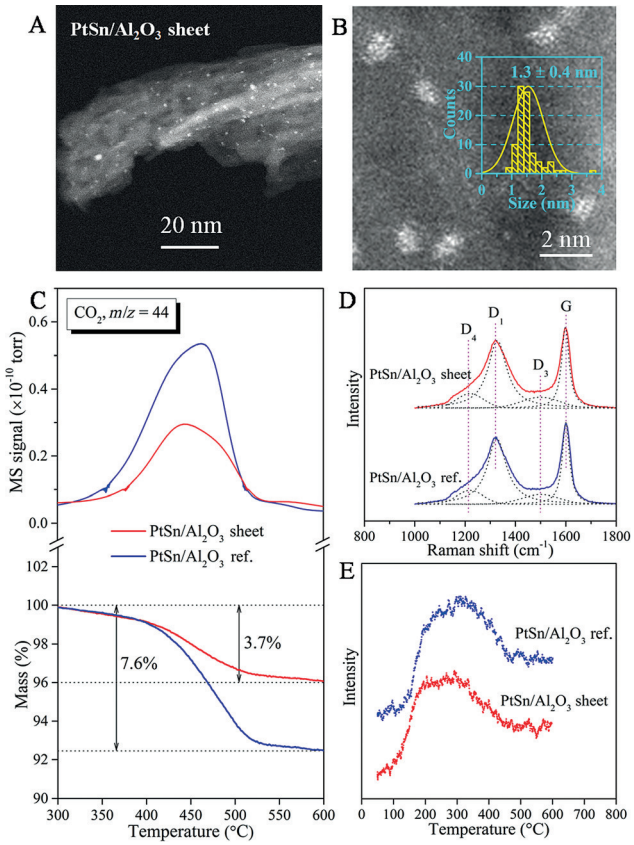

Figure 4. A, B) HAADF-STEM images of spent catalyst, inset: corresponding statistical analysis of the particle size distribution. C) Thermogravimetry (TG)-MS profiles under a TPO environment. D) Raman spectra of the spent catalysts. E) C_3H_6-TPD profiles of the fresh catalysts.

sites covered by coke is far smaller for the $PtSn/Al_2O_3$ sheet than for the $PtSn/Al_2O_3$ ref. catalyst. The temperature-programmed desorption of ammonia (C_3H_6-TPD; Figure 4E) profiles indicate that the interaction between the C_3H_6 molecules and the metal sites is weaker for the $PtSn/Al_2O_3$ sheet than for the $PtSn/Al_2O_3$ ref. catalyst. This weak interaction minimizes coke formation of the electron-rich C_3H_6 on the metal sites of the $PtSn/Al_2O_3$ sheet during reactions, which therefore remain highly stable under the reaction conditions.[19] These results account for the experimental observation that the $PtSn/Al_2O_3$ sheet catalyst was only slightly deactivated during a 24 h dehydrogenation reaction, whereas a dramatic deactivation was observed for the $PtSn/Al_2O_3$ ref. catalyst.

In conclusion, we have demonstrated that a γ-Al_2O_3 nanosheet that contains a large amount of pentacoordinate Al^{3+} ions is exceptionally able of dispersing and stabilizing Pt-Sn clusters. We could clarify that the electronic interactions between the two metals are enhanced on such a support, which leads to an increase in the electron density of the Pt sites. In the catalytic dehydrogenation of propane, this catalyst displayed an excellent specific activity for propylene formation with $>99\,\%$ selectivity, and did not suffer from coke formation or sintering processes. Our work has also demonstrated that the sheet construction of the catalyst facilitates mass-transfer and kinetically controlled diffusion processes during propane dehydrogenation.

Experimental Section

The Pt-Sn catalysts supported by Al_2O_3 nanosheets were prepared using the incipient co-impregnation method. Propane dehydrogenation was performed in a fixed-bed reactor with a feed consisting of $C_3H_8/H_2/N_2$ (1:1.25:4) under atmospheric pressure at 590 °C. The amount of deposited coke was determined by combustion of the deposited material on a thermogravimetric analyzer. For details, see the Supporting Information.

Acknowledgements

This study was supported by the National Natural Science Funds for Distinguished Young Scholars (21225312), the National Natural Science Foundation (21403027, 21373035, and U1462120), and the China Postdoctoral Science Foundation (2014M560202).

Keywords: alumina · dehydrogenation · heterogeneous catalysis · nanosheets · propane

How to cite: *Angew. Chem. Int. Ed.* **2015**, *54*, 13994–13998
Angew. Chem. **2015**, *127*, 14200–14204

[1] a) E. McFarland, *Science* **2012**, *338*, 340–342; b) J. L. He, T. Xu, Z. H. Wang, Q. H. Zhang, W. P. Deng, Y. Wang, *Angew. Chem. Int. Ed.* **2012**, *51*, 2438–2442; *Angew. Chem.* **2012**, *124*, 2488–2492.
[2] J. J. H. B. Sattler, J. Ruiz-Martinez, E. Santillan-Jimenez, B. M. Weckhuysen, *Chem. Rev.* **2014**, *114*, 10613–10653.
[3] J. A. Moulijn, A. E. van Diepen, F. Kapteijn, *Appl. Catal. A* **2001**, *212*, 3–16.
[4] K. J. Caspary, H. Gehrke, M. Heinritz-Adrian, M. Schwefer in *Handbook of Heterogeneous Catalysis*, *Vol. 6* (Eds.: G. Ertl, H. Knözinger, F. Schüth, J. Weitkamp), Wiley-VCH, Weinheim, **2008**, pp. 3206–3229.
[5] a) G. J. Siri, J. M. Ramallo-Lopez, M. L. Casella, J. L. G. Fierro, F. G. Requejo, O. A. Ferretti, *Appl. Catal. A* **2005**, *278*, 239–249; b) J. Y. Shen, J. M. Hill, R. M. Watwe, B. E. Spiewak, J. A. Dumesic, *J. Phys. Chem. B* **1999**, *103*, 3923–3934.
[6] J. H. Kwak, J. Z. Hu, D. Mei, C. W. Yi, D. H. Kim, C. H. F. Peden, L. F. Allard, J. Szanyi, *Science* **2009**, *325*, 1670–1673.
[7] a) Y. H. Liu, N. Zhao, H. Xian, Q. P. Cheng, Y. S. Tan, N. Tsubaki, X. G. Li, *ACS Appl. Mater. Interfaces* **2015**, *7*, 8398–8403; b) M. Choi, K. Na, J. Kim, Y. Sakamoto, O. Terasaki, R. Ryoo, *Nature* **2009**, *461*, 246–249; c) G. P. Hao, Z. Y. Jin, Q. Sun, X. Q. Zhang, J. T. Zhang, A. H. Lu, *Energy Environ. Sci.* **2013**, *6*, 3740–3747.
[8] a) Y. Li, W. J. Shen, *Chem. Soc. Rev.* **2014**, *43*, 1543–1574; b) L. Kovarik, A. Genc, C. M. Wang, A. N. Qiu, C. H. F. Peden, J. Szanyi, J. H. Kwak, *J. Phys. Chem. C* **2013**, *117*, 179–186; c) Y. Rozita, R. Brydson, T. P. Comyn, A. J. Scott, C. Hammond, A. Brown, S. Chauruka, A. Hassanpour, N. P. Young, A. I. Kirkland, H. Sawada, R. I. Smith, *ChemCatChem* **2013**, *5*, 2695–2706.
[9] S. A. Bradley, W. Sinkler, D. A. Blom, W. Bigelow, P. M. Voyles, L. F. Allard, *Catal. Lett.* **2012**, *142*, 176–182.
[10] a) D. Coster, A. L. Blumenfeld, J. J. Fripiat, *J. Phys. Chem.* **1994**, *98*, 6201–6211; b) X. J. Li, W. P. Zhang, S. L. Liu, L. Y. Xu, X. W. Han, X. H. Bao, *J. Catal.* **2007**, *250*, 55–66.

[11] C. Pecharromán, I. Sobrados, J. E. Iglesias, T. Gonzalez-Carreno, J. Sanz, *J. Phys. Chem. B* **1999**, *103*, 6160 – 6170.
[12] a) M. L. Yang, Y. A. Zhu, C. Fan, Z. J. Sui, D. Chen, X. G. Zhou, *Phys. Chem. Chem. Phys.* **2011**, *13*, 3257 – 3267; b) J. Singh, R. C. Nelson, B. C. Vicente, S. L. Scott, J. A. van Bokhoven, *Phys. Chem. Chem. Phys.* **2010**, *12*, 5668 – 5677.
[13] a) N. P. Lebedeva, A. Rodes, J. M. Feliu, M. T. M. Koper, R. A. van Santen, *J. Phys. Chem. B* **2002**, *106*, 9863 – 9872; b) P. Bazin, O. Saur, J. C. Lavalley, M. Daturi, G. Blanchard, *Phys. Chem. Chem. Phys.* **2005**, *7*, 187 – 194.
[14] A. Virnovskaia, S. Morandi, E. Rytter, G. Ghiotti, U. Olsbye, *J. Phys. Chem. C* **2007**, *111*, 14732 – 14742.
[15] A. Virnovskaia, S. Jørgensen, J. Hafizovic, Ø. Prytz, E. Kleimenov, M. Havecker, H. Bluhm, A. Knop-Gericke, R. Schlögl, U. Olsbye, *Surf. Sci.* **2007**, *601*, 30 – 43.
[16] J. C. Serrano-Ruiz, A. Sepulveda-Escribano, F. Rodriguez-Reinoso, *J. Catal.* **2007**, *246*, 158 – 165.
[17] P. P. Sun, G. Siddiqi, W. C. Vining, M. F. Chi, A. T. Bell, *J. Catal.* **2011**, *282*, 165 – 174.
[18] a) N. Martín, M. Viniegra, E. Lima, G. Espinosa, *Ind. Eng. Chem. Res.* **2004**, *43*, 1206 – 1210; b) J. F. Yu, R. Wang, S. Y. Ren, X. Y. Sun, C. L. Chen, Q. J. Ge, W. Fang, J. Zhang, H. Y. Xu, D. S. Su, *ChemCatChem* **2012**, *4*, 1376 – 1381.
[19] a) F. Jiang, L. Zeng, S. R. Li, G. Liu, S. P. Wang, J. L. Gong, *ACS Catal.* **2015**, *5*, 438 – 447; b) C. L. Yu, Q. J. Ge, H. Y. Xu, W. Z. Li, *Catal. Lett.* **2006**, *112*, 197 – 201.

Received: August 6, 2015
Published online: September 2, 2015

